

# Modeling the growth kinetics of a multi-component stoichiometric compound

Haifeng Wang · Feng Liu · D. M. Herlach

Received: 12 July 2013 / Accepted: 22 October 2013 / Published online: 8 November 2013  
© Springer Science+Business Media New York 2013

**Abstract** The maximal entropy production principle was applied to model the growth kinetics of a multi-component stoichiometric compound. Compared with the solid-solution phase and the non-stoichiometric compound, the dissipation by the trans-interface diffusion makes the interface slow down by decreasing the effective interface mobility and does not result in solute trapping or disorder trapping. An application to the crystallization of a CuZr stoichiometric compound shows that the transition from the thermodynamic-controlled to the kinetic-controlled growth can be predicted.

## Introduction

Most intermetallics and oxides are stoichiometric compounds (SCs) with no or extremely small solubility, i.e., line compounds. Modeling their growth kinetics is very important for not only solidification [1–7] but also solid-state phase transformations [8–16]. Recent work on some SC alloy systems (e.g., CuZr intermetallics [17, 18] and Al–Al<sub>3</sub>Sm eutectics [19, 20]), further shows that their abnormally slow growth behaviors upon solidification are quite useful for selecting the potential glass-forming systems.

The Gibbs energy of the SC in the thermodynamic databases is a concentration-independent constant at a given temperature  $T$ . For example, the molar Gibbs energy diagram for the solidification of a binary SC is shown in Fig. 1. The Gibbs energy and the concentration of the SC are  $g_s$  and  $C_s$ . The position of the SC (a point) in the diagram is denoted as the solid circle. By drawing the tangent of the liquid curve which goes through the solid circle (i.e., the common tangent rule), the equilibrium liquid concentration  $C_L^{eq}$  is determined. If the initial concentration  $C_0 = C_s$ , there are no solute diffusions in both the solid and the liquid and, the SC is crystallized like a pure element with the growth velocity  $V$  given by [21]:

$$V = V_0(T) \left[ 1 - \exp\left(\frac{\Delta g}{RT}\right) \right], \quad (1)$$

where the temperature-dependent  $V_0$  is the upper limit of  $V$ , and  $\Delta g$  is the driving free energy at the interface. If  $C_0 \neq C_s$ , the solute jump at the interface and the solute diffusion in the liquid happen. From the molar Gibbs energy diagram,  $\Delta g$  is the vertical distance from the solid circle to the tangent of the liquid curve at  $C_L^*$  [22] (The superscript “\*” denotes the values at the interface in the current work). The dissipations by the interface migration and the trans-interface diffusion cannot be distinguished from  $\Delta g$ , because there is no tangent for the SC.<sup>1</sup> In recent work of Wang et al. [19, 20], a semi-empirical power growth law was used to describe the kinetics of the Al<sub>3</sub>Sm SC upon eutectic solidification. Svoboda et al. [14–16] adopted the thermodynamic extremal principle (TEP)

---

H. Wang (✉) · F. Liu  
State Key Laboratory of Solidification Processing,  
Northwestern Polytechnical University, Xi’an 710072,  
Shaanxi, People’s Republic of China  
e-mail: haifengw81@nwpu.edu.cn

H. Wang · D. M. Herlach  
Institut für Materialphysik im Weltraum, Deutsches Zentrum für  
Luft- und Raumfahrt (DLR), 51170 Cologne, Germany

<sup>1</sup> For the solid-solution phase,  $\Delta g$  can be divided into the driving free energy for the interface migration  $\Delta g_C$  and the trans-interface diffusion  $\Delta g_D$  by moving the tangent of the solid curve at  $C_s$  to  $C_L^*$  in the liquid curve [22]; please see the two parallel dotted lines in Fig. 1.

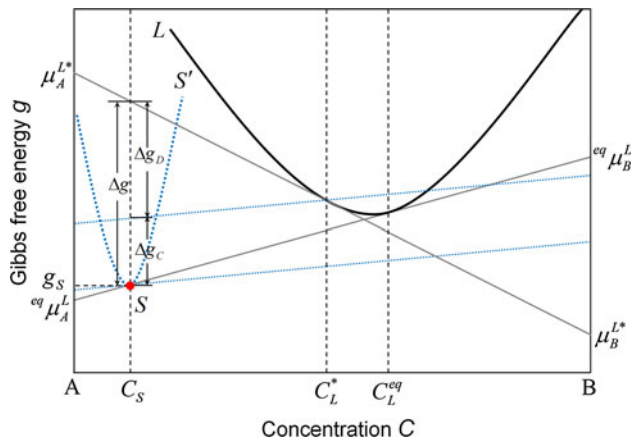


**Fig. 1** Molar Gibbs energy diagram for the crystallization of a binary stoichiometric compound. The position (a point) of the stoichiometric compound  $S$  ( $C_S, g_S$ ) is denoted as the *solid circle* and the concentration-dependent Gibbs energy of the liquid  $L$  is shown as the *thick solid line*. By drawing the tangent of the  $L$  curve that goes through the *solid circle* (i.e., the common tangent rule), the equilibrium liquid concentration  $C_L^{eq}$  and chemical potential  $^{eq}\mu_i^L$  ( $i = A$  or  $B$ ) are determined. Under non-equilibrium conditions where the liquid concentration is  $C_L^*$ , the driving free energy at the interface  $\Delta g$  and the non-equilibrium chemical potential  $\mu_i^{L*}$  ( $i = A$  or  $B$ ) are determined by drawing the tangent of the  $L$  curve at  $C_L^*$  [22].  $\Delta g$  is the vertical distance from the *solid circle* to the tangent. In the multi-phase field models [7, 9–13], a paraboloid Gibbs energy (e.g., the *dotted curve*  $S'$ ) is assumed to describe the kinetics of the stoichiometric compound by that of the solid-solution phase. The application of this approximation method, however, is rather limited [7]. For the solid-solution phase,  $\Delta g$  can be divided into the driving free energy for the interface migration  $\Delta g_C$  and the trans-interface diffusion  $\Delta g_D$  by moving the tangent of the  $S'$  curve at  $C_S$  to  $C_L^*$  in the  $L$  curve [22]. There is, however, no tangent of a point for the stoichiometric compound. In other words, the kinetics of the stoichiometric compound is essentially different from that of the solid-solution phase

[23–25] (i.e., a simplification of the maximal entropy production principle (MEPP) [26–28] to the linear thermodynamics) to model the stoichiometric precipitates in the binary and the multi-component alloy systems. However, all the work above does not show clearly the effect of the trans-interface diffusion on the growth kinetics of the SC. As is well-known, the trans-interface diffusion plays an important role in the growth kinetics of the solid-solution phase (SSP) and the non-stoichiometric compound (NSC), e.g., it makes the interface slow down by dissipating part of the driving free energy at the interface (i.e., the solute drag effect) and results in solute trapping or disorder trapping [22, 29–33].

The current work aims to develop a sharp interface model for the growth kinetics of the multi-component SC. Following our former work for the SSP [34–36], the MEPP was applied to formulate the model self-consistently in thermodynamics. The dissipation by the trans-interface diffusion was found to decrease the interface mobility considerably if

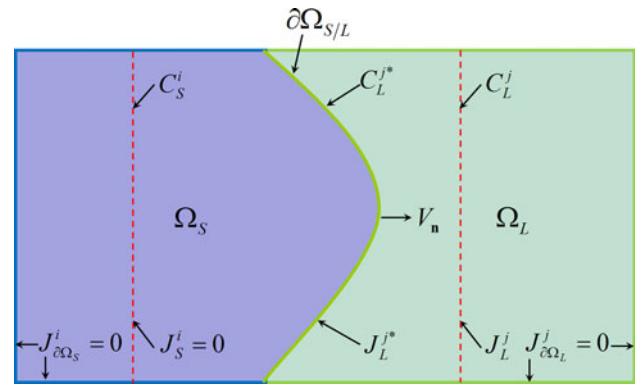


**Fig. 2** Schematic diagram for the crystallization of an  $n$ -component stoichiometric compound from an  $m$ -component undercooled melt ( $n \leq m$ ). The solid  $S$  ( $\Omega_S$ ) and the liquid  $L$  ( $\Omega_L$ ) are separated by a curved migrating  $S/L$  interface ( $\partial\Omega_{S/L}$ ) with a velocity  $\mathbf{V}_n$  in the normal direction of  $\partial\Omega_{S/L}$   $\mathbf{n}$ . Due to the invariable solid concentration  $C_S^i$  ( $i = 1, 2, \dots, n$ ), there are no solute fluxes in the solid, i.e.,  $J_S^i = 0$ . The liquid concentration and the solute fluxes in the liquid are denoted as  $C_L^j$  and  $J_L^j$  ( $j = 1, 2, \dots, m$ ) and,  $C_L^{j*}$  and  $J_L^{j*}$  are the values at the interface. For a closed system assumed here, there are no solute fluxes at the surfaces of the solid and the liquid, i.e.,  $J_{\partial\Omega_S}^i = J_{\partial\Omega_L}^j = 0$

the liquid concentration at the interface deviates much from the solid concentration. The growth kinetics of an undercooled CuZr SC was predicted and discussed.

**The model**

Let us consider a closed isothermal system in which an  $n$ -component SC is crystallized from an  $m$ -component undercooled melt ( $n \leq m$ ); please see Fig. 2. The solid  $S$  ( $\Omega_S$ ) and the liquid  $L$  ( $\Omega_L$ ) are separated by a curved  $S/L$  interface ( $\partial\Omega_{S/L}$ ). The growth velocity of the interface is  $\mathbf{V}_n$  with  $\mathbf{n}$  as the normal vector. For simplicity, the partial molar volumes of all the components in the solid and in the liquid are assumed to be equal ( $V_m$ ). If the local Gibbs energy of the bulk phases is denoted as  $g_k$  ( $k = S$  or  $L$ ) and the interface energy is a constant  $\sigma$ , the total Gibbs energy of the system  $G$  can be expressed as:

$$G = \sum_{k=S,L} \int_{\Omega_k} \frac{g_k}{V_m} d\Omega + \int_{\partial\Omega_{S/L}} \sigma d\Omega. \tag{2}$$

$g_S$  is only temperature-dependent due to the invariable solid concentration  $C_S^i$  ( $i = 1, 2, \dots, n$ ), whereas,  $g_L$  is not only temperature-dependent but also concentration-dependent:

$$g_L = \sum_{j=1}^m C_L^j \mu_L^j, \tag{3}$$

where  $C_L^j$  and  $\mu_L^j$  ( $j = 1, 2, \dots, m$ ) are the liquid concentration and the chemical potential, respectively.

Following the transport theorem [37], the rate of the total Gibbs energy change is obtained from Eq. (2) as

$$\dot{G} = \frac{1}{V_m} \left[ \int_{\Omega_L} \frac{\partial g_L}{\partial t} d\Omega - \int_{\partial\Omega_{S/L}} (g_L^* - g_S^* + \sigma KV_m) \mathbf{V}_n d\partial\Omega \right] \quad (4)$$

if there is no velocity field in the liquid. Here  $K$  is the interface curvature. The mass conservation law in the liquid is:

$$\frac{\partial C_L^j}{\partial t} = -V_m \nabla J_L^j, \quad (5)$$

where  $J_L^j$  is the diffusion flux. Regarding that there are no diffusion fluxes in the solid and at the surface of the solid and the liquid (i.e.,  $J_S^i = J_{\partial\Omega_S}^i = J_{\partial\Omega_L}^i = 0$ ), a combination of Eqs. (3)–(5) and the Gibbs–Duhem relation (i.e.,  $\sum_{j=1}^m C_L^j \partial \mu_L^j / \partial t = 0$ ) leads to:

$$\begin{aligned} \dot{G} = & \int_{\Omega_L} \sum_{j=1}^m J_L^j \nabla \mu_L^j d\Omega + \int_{\partial\Omega_{S/L}} \left\{ \sum_{j=1}^m (J_L^{j*} \mu_L^{j*}) \right. \\ & \left. - \frac{\mathbf{V}_n}{V_m} \left[ \sum_{j=1}^m (C_L^{j*} \mu_L^{j*}) - g^S + V_m \sigma K \right] \right\} d\partial\Omega \end{aligned} \quad (6)$$

The constraints among the diffusion fluxes in the liquid  $\sum_{j=1}^m J_L^j = 0$  and at the interface  $\sum_{j=1}^m J_L^{j*} = 0$  reduce Eq. (6) to

$$\begin{aligned} \dot{G} = & \int_{\Omega_L} \sum_{j=2}^m J_L^j \nabla (\mu_L^j - \mu_L^1) d\Omega + \int_{\partial\Omega_{S/L}} \left\{ \sum_{j=2}^m J_L^{j*} (\mu_L^{j*} - \mu_L^{1*}) \right. \\ & \left. - \frac{\mathbf{V}_n}{V_m} \left[ \sum_{j=1}^m (C_L^{j*} \mu_L^{j*}) - g^S + V_m \sigma K \right] \right\} d\partial\Omega \end{aligned} \quad (7)$$

Note that the component 1 is chosen here as the solvent.

For the bulk liquid, the Gibbs energy is dissipated by the flux of the solute diffusion  $J_L^j$ ; see the first term on the right hand of Eq. (7). For the interface, the Gibbs energy is dissipated by the fluxes of the trans-interface diffusion  $J_D^j = J_L^{j*}$  [34] and the interface migration  $J_C = \mathbf{V}_n / V_m$  [22]; see the second term on the right hand of Eq. (7). Therefore, the total Gibbs energy dissipation  $Q$  can be according to the TEP [23–25] given by:

$$Q = \int_{\Omega_L} \sum_{j=2}^m \frac{J_L^j{}^2}{M_{J_L^j}} d\Omega + \int_{\partial\Omega_{S/L}} \left[ \sum_{j=2}^m \frac{J_D^j{}^2}{M_{J_D^j}} + \frac{J_C^2}{M_{J_C}} \right] d\partial\Omega \quad (8)$$

where  $M_{J_L^j}$ ,  $M_{J_D^j}$ , and  $M_{J_C}$  are the mobilities of the solute diffusion, the trans-interface diffusion, and the interface migration [21, 25, 34–36]:

$$\begin{aligned} M_{J_L^j} &= \frac{D_L^j}{V_m} \frac{\partial C_L^j}{\partial (\mu_L^j - \mu_L^1)} \approx \frac{D_L^j}{V_m RT} \frac{C_L^j C_L^1}{(C_L^j + C_L^1)}, \\ M_{J_D^j} &= \frac{D_L^{j*}}{a_0 V_m} \frac{\partial C_L^{j*}}{\partial (\mu_L^{j*} - \mu_L^{1*})} \approx \frac{D_L^{j*}}{a_0 V_m RT} \frac{C_L^{j*} C_L^{1*}}{(C_L^{j*} + C_L^{1*})}, \\ M_{J_C} &= \frac{V_0(T)}{RTV_m} \end{aligned} \quad (9)$$

Here  $D_L^j$  and  $D_L^{j*}$  are the diffusion coefficients, and  $a_0$  is the interatomic spacing.

According to the transport theorem [37], the mass conservation law (or the jump condition) at the interface is:

$$J_L^{j*} = \frac{V_n (C_L^{j*} - C_S^i \delta_{ij})}{V_m}, \quad (10)$$

where the Dirac delta function  $\delta_{ij}$  is introduced because there are no redundant components from  $n + 1$  to  $m$  in the solid. Eq. (10) is actually an additional constraint in the system that should be considered during the application of the TEP (or the MEPP). The evolution of the system according to the TEP [23–25] follows<sup>2</sup>:

$$\delta \left\{ \dot{G} + \frac{1}{2} Q + \int_{\partial\Omega_{S/L}} \sum_{j=2}^m \lambda_j \left[ J_L^{j*} - \frac{V_n}{V_m} (C_L^{j*} - C_S^i \delta_{ij}) \right] d\partial\Omega \right\} = 0, \quad (11)$$

where  $\lambda_j$  is the associated Lagrange multiplier. Then, substituting Eqs. (7) and (8) into Eq. (11) and eliminating  $\lambda_j$  yield the diffusion equation in the liquid (i.e., the classical Fick’s law):

$$J_L^j = -M_{J_L^j} \nabla (\mu_L^j - \mu_L^1) = -\frac{D_L^j}{V_m} \nabla C_L^j \quad (12)$$

and the growth kinetics of the interface:

$$\begin{aligned} J_C = \frac{V_n}{V_m} = & - \left[ \frac{1}{M_{J_C}} + \sum_{j=2}^m \frac{(C_L^{j*} - C_S^i \delta_{ij})^2}{M_{J_D^j}} \right]^{-1} \\ & \times \left[ g^S - \sum_{j=1}^n (C_S^j \mu_L^{j*}) - V_m \sigma K \right]. \end{aligned} \quad (13)$$

Even if the redundant components in the liquid have no contributions to the driving free energy at the interface, their trans-interface diffusion fluxes influence on the effective interface mobility  $M_{J_C}^{\text{eff}} = [1/M_{J_C} + \sum_{j=2}^m (C_L^{j*} - C_S^i \delta_{ij})^2 / M_{J_D^j}]^{-1}$ . Because  $M_{J_C}^{\text{eff}} < M_{J_C}$ , the trans-interface diffusion, like the solute drag effect in the SSP and the NSC, makes the

<sup>2</sup> The driving free energy for each dissipation process cannot be self-derived by the MEPP for the nonlinear thermodynamics and needs to be prescribed by the TEP or the molar Gibbs energy diagram [34].

interface slow down. If the MEPP for the non-linear thermodynamics [34] is adopted, the growth kinetics can be obtained as:

$$\mathbf{V}_n = \left[ \frac{1}{V_0} + \sum_{j=2}^m \frac{a_0}{D_L^{j*}} \frac{(C_L^{j*} + C_L^{1*})(C_L^{j*} - C_S^i \delta_{ij})^2}{C_L^{j*} C_L^{1*}} \right]^{-1} \times \left\{ 1 - \exp \left[ \frac{g^S - \sum_{j=1}^n (C_S^j \mu_L^{j*}) - V_m \sigma K}{RT} \right] \right\}, \quad (14)$$

where the first and the second terms on the right hand are the kinetic and the thermodynamic contributions, respectively. When  $n = m$  and the initial concentration  $C_L^{i0} = C_S^i$ , Eq. (14) reduces to Eq. (1) in the case of planar solidification. The effective upper limit of growth velocity  $V_0^{\text{eff}} = V_0$  is only temperature-dependent. Otherwise,  $V_0^{\text{eff}} = V_m R T M_{j_c}^{\text{eff}}$  is not only temperature-dependent but also concentration-dependent. Under equilibrium conditions ( $V = 0$ ), Eq. (14) reduces to  $g^S - \sum_{j=1}^n (C_S^j \mu_L^{j*}) - V_m \sigma K = 0$ , which is the Gibbs–Thomson equation for the multi-component SC [38, 39].

### Application to the crystallization of a CuZr stoichiometric compound

The current interface kinetic model (Eq. 14) is applied to the crystallization of the CuZr SC from a binary Cu–Zr glass-forming alloy system. The driving free energy at the interface is obtained from the CALPHAD thermodynamic assessment by Wang et al. [40]. The interface mobility is generally assumed to be temperature-dependent and concentration-dependent through the diffusion coefficient, the viscosity, and so on [21, 41]. Following Aziz and Boettinger [21], the interface mobility is currently assumed to depend linearly on the diffusion coefficient in the liquid, i.e.,  $V_0 = f D_L / a_0$  with  $f$  as a geometrical factor of order unity. This assumption is consistent with the recent molecular dynamics simulations by Tang and Harrowell [18] and is helpful for understanding the transition from the thermodynamic-controlled to the kinetic-controlled growth in undercooled melts [41, 42].

#### Kinetic phase diagram

The kinetic phase diagram for the crystallization of the CuZr SC is calculated by setting  $V_0 = f D_L / a_0 = 1425.8 \exp(-79759/RT)$  and  $V_{Dl} = D_L^* / a_0 = V_0 / 2$  ( $\text{m s}^{-1}$ ); please see Fig. 3. The thin solid lines are the equilibrium liquidus and its extension (below the two star symbols).

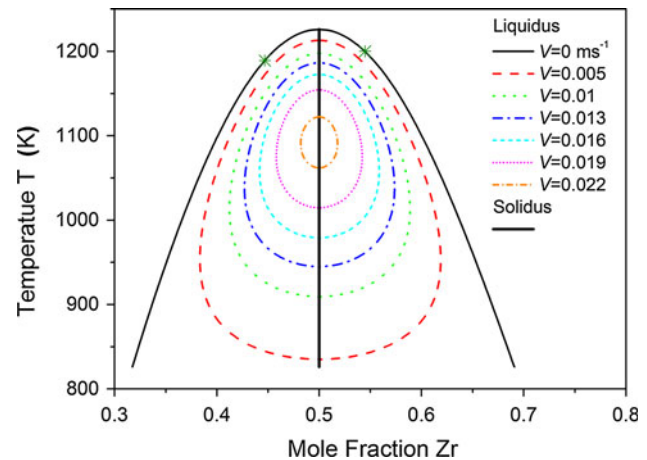


**Fig. 3** Equilibrium ( $V = 0$ ) and non-equilibrium ( $V \neq 0$ ) phase diagrams for the crystallization of a CuZr stoichiometric compound. Below the two stars is the extension of the equilibrium liquidus. Under non-equilibrium conditions ( $V \neq 0$ ), the liquid concentration deviates from the equilibrium concentration to provide the driving free energy at the interface. For a given  $V$ , the deviation needs to increase gradually to provide more thermodynamic contribution as the decrease of  $T$  because of the continuous decrease of the kinetic contribution. The kinetic liquidus therefore bends toward to the solidus at low  $T$  to show itself as an egg shape

The thick vertical solid line is the equilibrium solidus. Under non-equilibrium conditions, the liquid concentration deviates from the equilibrium concentration to provide the driving free energy at the interface. For a given  $V$ , the deviation needs to increase gradually to provide more thermodynamic contribution as the decrease of  $T$  because of the continuous decrease of the kinetic contribution. The kinetic liquidus therefore bends toward to the solidus at low  $T$  and shows itself as an egg shape. As the increase of  $V$ , the kinetic liquidus becomes smaller and smaller and its maximal temperature at  $C_L = 0.5$  decreases gradually. When  $V$  approaches its maximal value  $0.0227 \text{ m s}^{-1}$ , the kinetic liquidus and solidus converge to the point ( $C_L = 0.5$ ,  $T = 1094.6 \text{ K}$ ). The kinetic phase diagram implies that there is a critical interface temperature below which the growth velocity begins to decrease for a given  $C_L^*$ , i.e., the transition from the thermodynamic-controlled to the kinetic-controlled growth.

#### Transition from the thermodynamic-controlled to the kinetic-controlled growth

To show the transition more clearly, the evolution of  $V$  with the interface undercooling  $\Delta T_1$  is calculated for a fixed  $C_L^*$ ; please see the lines in Fig. 4. The concentrations chosen are on the right side of the solidus in Fig. 3. Independent on  $C_L^*$ ,  $V$  increases firstly and then decreases as the increase of  $\Delta T_1$ . The maximal velocity  $V^{\text{max}}$  decreases gradually as the increase of  $C_L^*$  and so is the

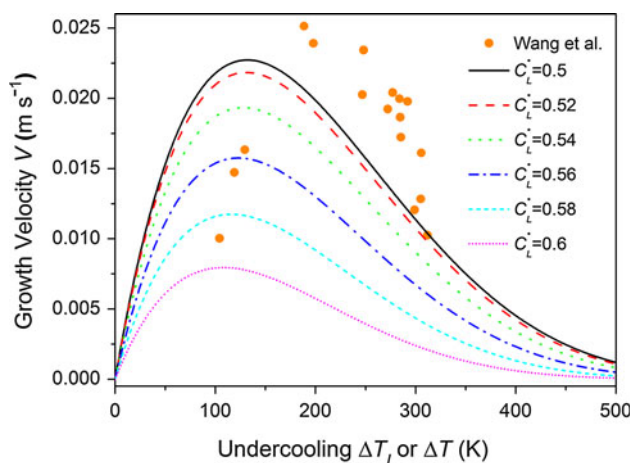


**Fig. 4** Evolution of the growth velocity  $V$  with the interface undercooling  $\Delta T_I$  for a fixed liquid concentration at the interface  $C_L^*$ . The  $V \sim \Delta T$  relation measured by Wang et al. [17] is shown as the solid circles. The experimental results can be well reproduced if the current growth kinetic model is incorporated into the dendrite growth theory to consider the contributions of the thermal and the curvature undercooling to  $\Delta T$

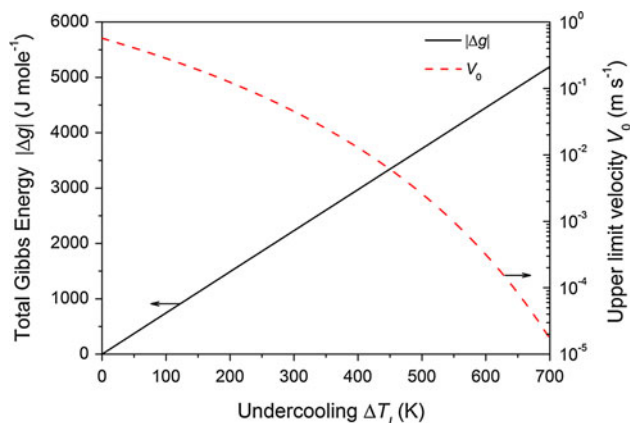


**Fig. 5** Evolution of the absolute value of the driving free energy at the interface  $|\Delta g|$  and the upper limit of growth velocity  $V_0$  with the interface undercooling  $\Delta T_I$  for  $C_L^* = 0.5$ . A continuous increase of the thermodynamic contribution  $|\Delta g|$  is followed by a constant decrease of the kinetic contribution  $V_0$ , thus resulting in the transition from the thermodynamic-controlled to the kinetic-controlled growth

corresponding interface undercooling  $\Delta T_I^\wedge$ . Since an increase of  $C_L^*$  from 0.5 to 0.6 makes the maximal point decrease from ( $V^{\max} = 0.0227 \text{ m s}^{-1}$ ,  $\Delta T_I^\wedge = 132.2 \text{ K}$ ) to ( $V^{\max} = 0.008 \text{ m s}^{-1}$ ,  $\Delta T_I^\wedge = 108.15 \text{ K}$ ), the effect of the trans-interface diffusion on the growth kinetics of the SC could be significant. Similar calculation results are obtained if the concentrations chosen are on the left side of the solidus.

The physics behind the transition is that there is a competition between the driving free energy from the thermodynamics and the interface mobility from the kinetics. Figure 5 shows the evolution of  $|\Delta g| =$

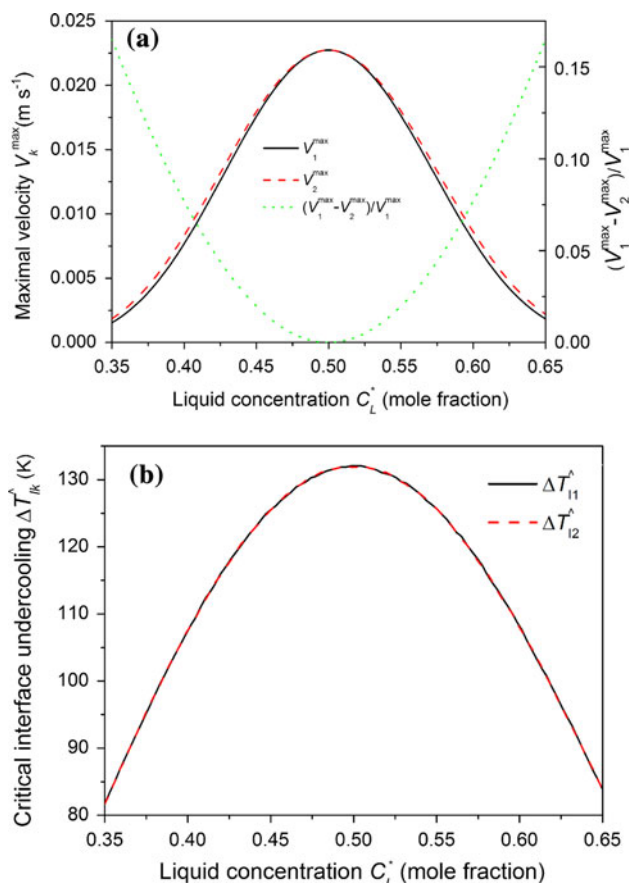


**Fig. 6** Evolution of the maximal velocity  $V_k^{\max}$  (a) and the corresponding critical interface undercooling  $\Delta T_{ik}^\wedge$  (b) with the liquid concentration at the interface  $C_L^*$ .  $k = 1$  and  $2$  correspond to the case with ( $V_{DI} = V_0/2$ ) and without ( $V_{DI} = \infty$ ) the effect of trans-interface diffusion, respectively. The relative differences in  $V_k^{\max}$  between the two cases are shown as the dotted line in Fig. 6a. The differences between  $\Delta T_{i1}^\wedge$  and  $\Delta T_{i2}^\wedge$  are indistinguishable in b

$|g^S - C_S \mu_L^{Zr} - (1 - C_S) \mu_L^{Cu}|$  and  $V_0$  with  $\Delta T_I$  for  $C_L^* = 0.5$ . As the increase of  $\Delta T_I$ ,  $|\Delta g|$  increases continuously,  $V_0$  decreases constantly. Therefore, the thermodynamics dominates initially, and  $V$  increases with  $\Delta T_I$ . After that the kinetics becomes more and more dominant and finally results in the decrease of  $V$  with  $\Delta T_I$ . Consequently, a transition from the thermodynamic-controlled to the kinetic-controlled growth happens for the crystallization of the CuZr SC.

To show the effect of the trans-interface diffusion on the transition, the evolution of  $V_k^{\max}$  ( $k = 1$  and  $2$  correspond to the case with ( $V_{DI} = V_0/2$ ) and without ( $V_{DI} = \infty$ ) the effect of the trans-interface diffusion, respectively) and  $\Delta T_{ik}^\wedge$  with  $C_L^*$  is calculated; please see Fig 6a, b. As the increase of the deviation of  $C_L^*$  from  $C_S = 0.5$ ,  $V_k^{\max}$  decreases continuously and so is  $\Delta T_{ik}^\wedge$ . The differences between the two cases are neglectable for  $\Delta T_{ik}^\wedge$  but not for  $V_k^{\max}$ , e.g., a deviation of 0.15 for  $C_L^*$  from  $C_S = 0.5$  makes

$V^{\max}$  decrease by more than 15 % (the dotted line in Fig. 6a). In other words, the trans-interface diffusion plays an important role in the kinetics of not only the SSP and the NSC but also the SC if the deviation of the liquid concentration at the interface from the solid concentration is significant.

Compared with the experimental results in an undercooled  $\text{Cu}_{50}\text{Zr}_{50}$  melt

$\text{Cu}_{50}\text{Zr}_{50}$  alloy was undercooled by electrostatic levitation to measure the growth velocity  $V$  as function of undercooling  $\Delta T$  [17]. It was found that  $V$  increases firstly and then decreases with  $\Delta T$ ; please see the solid circles in Fig. 4. Tang and Harrowell [18] reported similar results for the isothermal crystallization of the CuZr SC using the molecular dynamics simulation. Although such an abnormal  $V \sim \Delta T$  relation is quite different from our general understanding of the undercooled metallic melts in which  $V$  always increases with  $\Delta T$  [43], it was frequently observed experimentally in the organic, the inorganic and the polymeric systems [41, 42]. A viscosity-dependent  $V_0$  proposed by fitting with the experimental results in the organic and the inorganic but not the metallic systems [41] was adopted by Wang et al. [17] to predict the  $V \sim \Delta T$  relation. Although  $V^{\max} = 0.025 \text{ m s}^{-1}$  was reproduced, a large deviation of 127 K from the corresponding undercooling  $\Delta T^{\wedge} = 200 \text{ K}$  (the solid circles in Fig. 4) was found. Our work for  $C_L^* = 0.5$  (i.e., the crystallization of the CuZr SC from the undercooled  $\text{Cu}_{50}\text{Zr}_{50}$  melt) shows that  $V^{\max} = 0.0227 \text{ m s}^{-1}$  at  $\Delta T_1^{\wedge} = 132 \text{ K}$ ; please see Fig. 4.  $V^{\max}$  is also predicted and the difference between  $\Delta T_1^{\wedge}$  and  $\Delta T^{\wedge}$  68 K is nearly two times smaller than that of Wang et al. [17] 127 K. The experimental results can be well predicted if the current growth kinetic model is incorporated into the dendrite growth theory (e.g., [44, 45]) to consider the contributions of the thermal and the curvature undercoolings to  $\Delta T$ .

## Conclusions

A thermodynamically consistent growth kinetic model was developed for the multi-component SC based on the MEPP (the TEP). In contrast to the kinetics of the SSP and the NSC, there is only one interface condition for the SC [Eq. (13) or (14)]. If the initial concentration is same as the SC, the Gibbs free energy at the interface is totally dissipated by the interface migration. Otherwise, it is dissipated by both the interface migration and the trans-interface diffusion. The trans-interface diffusion makes the interface slow down by decreasing the interface mobility and it does not result in solute trapping or disorder trapping. The

dissipation by the trans-interface diffusion cannot be separated from the driving free energy at the interface. Adopting the linearly diffusion coefficient-dependent interface mobility of Aziz and Boettinger [21], the transition from the thermodynamic-controlled to the kinetic-controlled growth during the crystallization of the CuZr SC was predicted.

It must be pointed out that a paraboloid Gibbs energy<sup>3</sup> is usually introduced to ensure the correct equilibrium conditions and a minimal solubility in the SC to satisfy the equal diffusion potential conditions in the multi-phase field models [11]; please see the dotted line in Fig. 1 ( $S'$ ). By this way, the growth kinetics of the SC can be described by that of the SSP. The curvature of the paraboloid must be chosen carefully to fit the Gibbs energy of the SC and avoid any unreasonable simulation result. Although widely used [7, 9–13], this approximation method is limited to near-equilibrium conditions with weak Gibbs–Thomson effect [11]. The current work shows that the growth kinetics of the SSP and the SC are essentially different and thus the multi-phase field model for the SC needs to be re-derived self-consistently in thermodynamics (e.g., by the MEPP [36]).

**Acknowledgements** Haifeng Wang would like to thank the support of Alexander von Humboldt Foundation for a research fellowship. Haifeng Wang and Feng Liu are grateful to the National Basic Research Program of China (973 Program, No. 2011CB610403), the National Science Funds for Distinguished Young Scientists (No. 51125002), the Natural Science Foundation of China (Nos. 51371149, 51101122 and 51071127), the NSFC-RFBR Collaboration Project (No. 512111059), the Aeronautical Science Foundation of China (No. 2011ZF53067), and the 111 Project (No. B08040) of Northwestern Polytechnical University. Financial support by Deutsche Forschungsgemeinschaft within the contract HE1601/26 is gratefully acknowledged by D.M. Herlach.

## References

1. Artini C, Muolo ML, Passerone A et al (2013) Isothermal solid–liquid transitions in the (Ni, B)/ZrB<sub>2</sub> system as revealed by sessile drop experiments. *J Mater Sci* 48:5029–5035. doi:10.1007/s10853-013-7290-0
2. Shuleshova O, Löser W, Holland-Moritz D et al (2012) Solidification and melting of high temperature materials: in situ observations by synchrotron radiation. *J Mater Sci* 47:4497–4513. doi:10.1007/s10853-011-6184-2
3. Kugler K, Ravlich I, Jones MI (2012) Effects of amount and type of cation species on the phase formation of single and codoped  $\alpha$ -SiAlONs. *J Mater Sci* 47:1205–1216. doi:10.1007/s10853-011-5697-z
4. Krivilyov M, Volkmann T, Gao J et al (2012) Multiscale analysis of the effect of competitive nucleation on phase selection in rapid solidification of rare-earth ternary magnetic materials. *Acta Mater* 60:112–122

<sup>3</sup> The Gibbs free energy as a function of the concentration follows the parabola function.

5. Wang CH, Kuo CY (2011) Interfacial reactions between eutectic Sn–Pb solder and Co substrate. *J Mater Sci* 46:2654–2661. doi:10.1007/s10853-010-5121-0
6. Hermann R, Bäcker I (2000) Growth kinetics in undercooled Nd–Fe–B alloys with carbon and Ti or Mo additions. *J Mag Mater* 213:82–86
7. Heulens J, Blanpain B, Moelans N (2011) A phase field model for isothermal crystallization of oxide melts. *Acta Mater* 59:2156–2165
8. Yamada T, Miura K, Kajihara M et al (2004) Formation of intermetallic compound layers in Sn/Au/Sn diffusion couple during annealing at 433 K. *J Mater Sci* 39:2327–2334. doi:10.1016/j.jallcom.2009.04.077
9. Li DY, Chen LQ (1998) Computer simulation of stress-oriented nucleation and growth of  $\theta'$  precipitates in Al–Cu alloys. *Acta Mater* 46: 2573–2585
10. Vaithyanathan V, Wolverton C, Chen LQ (2002) Multiscale modeling of precipitate microstructure evolution. *Phys Rev Lett* 88:125503
11. Hu SY, Murray J, Weiland H et al (2007) Thermodynamic description and growth kinetics of stoichiometric precipitates in the phase-field approach. *Calphad* 31:303–312
12. Kim HS, Lee HJ, Yu YS et al (2009) Three-dimensional simulation of intermetallic compound layer growth in a binary alloy system. *Acta Mater* 57:1254–1262
13. Ramdan RD, Takaki T, Tomita Y (2008) Free energy problem for the simulations of the growth of Fe<sub>2</sub>B phase using phase-field method. *Mater Trans* 49:2625–2631
14. Svoboda J, Gamsjäger E, Fischer FD (2006) Influence of diffusional stress relaxation on growth of stoichiometric precipitates in binary systems. *Acta Mater* 54:4575–4581
15. Svoboda J, Fischer FD, Abart R (2011) Modeling of diffusional phase transformation in multi-component systems with stoichiometric phases. *Acta Mater* 58:2905–2911
16. Svoboda J, Fischer FD, Schillinger W (2013) Formation of multiple stoichiometric phases in binary systems by combined bulk and grain boundary diffusion: experiments and model. *Acta Mater* 61:32–39
17. Wang Q, Wang LM, Ma MZ et al (2011) Diffusion-controlled crystal growth in deeply undercooled melt on approaching the glass transition. *Phys Rev B* 83:014202
18. Tang CG, Harrowell P (2013) Anomalously slow crystal growth of the glass-forming alloy CuZr. *Nat Mater* 12:507–511
19. Wang N, Kalay YE, Trivedi R (2011) Eutectic-to-metallic glass transition in the Al–Sm system. *Acta Mater* 59:6604–6619
20. Trivedi R, Wang N (2012) Theory of rod eutectic growth under far-from-equilibrium conditions: nanoscale spacing and transition to glass. *Acta Mater* 60:3140–3152
21. Aziz MJ, Boettinger WJ (1994) On the transition from short-range diffusion-limited to collision-limited growth in alloy solidification. *Acta Metall Mater* 42:527–537
22. Hillert M (1999) Solute drag, solute trapping and diffusional dissipation of Gibbs energy. *Acta Mater* 47:4481–4505
23. Svoboda J, Turek I (1991) On diffusion-controlled evolution of closed solid-state thermodynamic systems at constant temperature and pressure. *Philos Mag B* 64:749–759
24. Svoboda J, Turek I, Fischer FD (2005) Application of the thermodynamic extremal principle to modeling of thermodynamic processes in material sciences. *Philos Mag* 85:3699–3707
25. Svoboda J, Fischer FD, Fratzl P et al (2002) Diffusion in multi-component systems with no or dense sources and sinks for vacancies. *Acta Mater* 50:1369–1381
26. Onsager L (1931) Reciprocal relations in irreversible processes. I. *Phys Rev* 37:405–426
27. Ziegler H (1983) An introduction to thermodynamics. North-Holland, Amsterdam
28. Martyushev LM, Seleznev VD (2006) Maximum entropy production principle in physics, chemistry and biology. *Phys Rep* 426:1–45
29. Aziz MJ (1982) Model for solute redistribution during rapid solidification. *J Appl Phys* 53:1158–1168
30. Aziz MJ, Kaplan T (1988) Continuous growth model for interface motion during alloy solidification. *Acta Metall* 36:2335–2347
31. Boettinger WJ, Aziz MJ (1989) Theory for the trapping of disorder and solute in intermetallic phases by rapid solidification. *Acta Mater* 37:3379–3391
32. Assadi H, Greer AL (1996) Site-ordering effects on element partitioning during rapid solidification of alloys. *Nature* 383:150–152
33. Assadi H (2007) A phase-field model for non-equilibrium solidification of intermetallics. *Acta Mater* 55:5225–5235
34. Wang HF, Liu F, Zhai HM et al (2012) Application of the maximal entropy production principle to rapid solidification: a sharp interface model. *Acta Mater* 60:1444–1454
35. Wang K, Wang HF, Liu F et al (2013) Modeling rapid solidification of multi-component concentrated alloys. *Acta Mater* 61:1359–1372
36. Wang HF, Liu F, Ehlen GJ et al (2013) Application of the maximal entropy production principle to rapid solidification: a multi-phase-field model. *Acta Mater* 61:2617–2627
37. Fischer FD, Simha NK (2004) Influence of material flux on the jump relations at a singular interface in a multicomponent solid. *Acta Mech* 171:213–223
38. Du Q, Perez M, Poole WJ et al (2012) Numerical integration of the Gibbs–Thomson equation for multicomponent systems. *Scr Mater* 66:419–422
39. Shahandeh S, Nategh S (2007) A computational thermodynamics approach to the Gibbs–Thomson effect. *Mater Sci Eng A* 443: 178–184
40. Wang N, Li CR, Du ZM et al (2006) The thermodynamic re-assessment of the Cu–Zr system. *Calphad* 30:461–469
41. Ediger MD, Harrowell P, Yu L (2008) Crystal growth kinetics exhibit a fragility-dependent decoupling from viscosity. *J Chem Phys* 128:034709
42. Shun Y, Xi HM, Chen S et al (2008) Crystallization near glass transition: transition from diffusion-controlled to diffusionless crystal growth studied with seven polymorphs. *J Phys Chem B* 112:5594–5601
43. Herlach DM (1994) Non-equilibrium solidification of undercooled metallic metals. *Mater Sci Eng R* 12:177–272
44. Wang HF, Liu F, Chen Z et al (2007) Analysis of non-equilibrium dendrite growth in a bulk undercooled alloy melt: model and application. *Acta Mater* 55:497–506
45. Wang K, Wang HF, Liu F et al (2013) Modeling dendrite growth in undercooled concentrated multi-component alloys. *Acta Mater* 61:4254–4265